Infinite Phased-Array Analysis Using FDTD Periodic Boundary Conditions—Pulse Scanning in Oblique Directions

Henrik Holter and Hans Steyskal, *Fellow, IEEE*

***Abstract*— Unit cell analysis of infinite phased arrays in the finite difference time domain (FDTD) is performed by implementation of periodic boundary conditions. The technique allows for pulse excitation and oblique scan directions in both the cardinal and intercardinal planes. To our knowledge, this is the first paper presenting FDTD computations for intercardinal pulse scanning in oblique directions. The ordinary Yee lattice is used, which makes the algorithm easy to incorporate in an already existing FDTD code. Nonperiodic boundaries are truncated by Berenger's perfectly matched layer (PML). Active impedance of an infinite dipole array is calculated with the new method and validation is performed via the "element-by-element" approach, i.e., by a conventional FDTD simulation of a corresponding large finite array. Excellent agreement is found and the technique has been numerically stable in all cases analyzed.**

***Index Terms*—FDTD, numerical analysis, periodic structures, phased array.**

I. Introduction

MANY geometries in electromagnetic problems have an infinite periodic structure in one or two dimensions. In the frequency domain, the mathematical treatment of such structures is greatly simplified by Floquet's theorem, which reduces the analysis to that of a single unit cell in the structure [1]. Infinite phased-array analysis belongs to this class of problems. The analysis of infinite periodic arrays is important for understanding the electromagnetic behavior of elements in large finite arrays.

The finite-difference time-domain method (FDTD) is well suited for antenna analysis. The geometry and material modeling capability make FDTD especially suited for advanced antenna element development, the wide-band data generation is especially appropriate for broad-band antennas and the near-field data generation is important for impedance calculation, visualization, etc. Therefore, it is most desirable to develop also a time-domain analogy of Floquet's theorem.

A number of papers dealing with periodic boundary conditions in FDTD have been published (see, e.g., [2]–[12]). However, the few papers that consider the case of pulse excitation and oblique scan directions appear to be approximate or complicated to implement numerically [2]–[5]. Our earlier short letter treats pulse scanning in oblique directions in the cardinal planes for one-dimensional (1-D) and two-dimensional (2-D) arrays [13]. The purpose of the present paper is twofold. First, and most important, it generalizes our earlier technique to pulse scanning in intercardinal planes. Second, the cardinal plane scanning technique is more thoroughly explained. To our knowledge, this is the first paper presenting a FDTD analysis for pulse scanning in intercardinal planes.

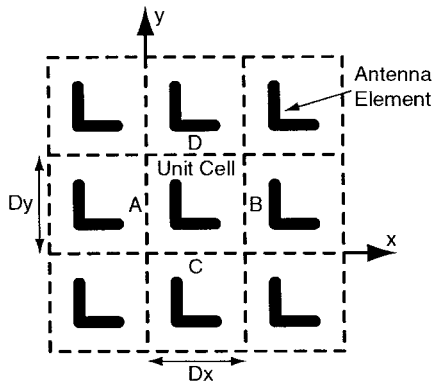

Fig. 1. Top view of the infinite periodic array.

II. The Problem of Unit-Cell Analysis in FDTD

Unit-cell analysis in the time domain is difficult for the following reason. Consider a unit cell with dimension $D_x \times D_y$ in an infinite periodic array, as shown in Fig. 1, and assume that the array is scanned in the $y = 0$ plane to an angle θ in the positive x direction. The fields at boundary C and D are then identical at every instant of time. Therefore, simple time independent boundary conditions can be applied. However, at boundaries A and B the tangential fields are related according to

$$f(x_B, y, z, t) = f(x_A, y, z, t - \tau_x) \tag{1}$$

$$f(x_A, y, z, t) = f(x_B, y, z, t + \tau_x) \tag{2}$$

where $f(x, y, z, t)$ is one of the tangential components of the electric or magnetic field.

$$\tau_x = \frac{D_x \sin\theta}{c} \tag{3}$$

Manuscript received September 14, 1998.

H. Holter is with the Department of Electromagnetic Theory, Royal Institute of Technology, Stockholm, S-100-44 Sweden.

H. Steyskal is with the Air Force Research Laboratory (formerly Rome Air Development Center), Hanscom AFB, 01731-3010 MA, and with the Department of Electromagnetic Theory, Royal Institute of Technology, Stockholm, S-100-44 Sweden.

Publisher Item Identifier S 0018-926X(99)09381-3.

is the excitation time delay between adjacent unit cells and c is the speed of light. Equation (1) implies that tangential field values at boundary B are obtained from time-delayed values at boundary A, which are simply saved in a buffer for later use. On the other hand (2), implies that time-advanced field values from boundary B are used at boundary A. This poses a major problem since the time advanced values at time $t+\tau_x$ are not known at time t.

III. Formulation of the Technique

In this section, the technique for oblique pulse scanning is formulated. The first subsection treats scanning in the cardinal planes. This is a more detailed explanation of the method presented earlier by us in a short letter [13]. In the second subsection, intercardinal plane scanning is considered. The techniques will be explained mainly by two examples. In both cases of cardinal and intercardinal scanning, there is no restriction on the size of the FDTD Yee cell, the cell dimension Δx, Δy, and Δz may be chosen arbitrarily. However, the numerical time step Δt is somewhat dependent on the size of the unit cell. Furthermore, the number of possible scan angles is a discrete number, which increases with increasing spatial resolution of the FDTD volume.

A. Cardinal Plane Scanning

First, the technique for pulse scanning of a 1-D array is explained, where afterward the method is extended to a 2-D array scanned in a cardinal plane.

Consider the 1-D linear infinite array in Fig. 2 and assume that the array is scanned to an angle θ so that the pulse excitation appears to move with the phase velocity $c/\sin\theta$ along the array. The dashed rectangle represents a three-dimensional (3-D) unit cell modeled in FDTD. The idea is now to move this cell with the speed of light in the x direction. This is accomplished by shifting the FDTD volume in the computer memory, which is a fast operation. An observer moving with the cell sees no field with motion in the positive x direction but only sees a field entering the unit cell at boundary B and leaving the cell at boundary A (and boundary C and D in Fig. 1). Thus, the fields radiating from the infinitely many array elements to the left of boundary A will never reach the moving cell. Normally, the FDTD method requires some kind of boundary condition to truncate the finite computational volume. However, with our technique, no boundary condition needs to be fulfilled on boundary A. Reflections from boundary A will never catch up with the moving unit cell, so boundary A need not be considered. The effect is that the boundary condition represented by (2) is unnecessary. At boundary B time-delayed values obtained from an earlier time point in the FDTD computation are applied.

1) Example: With reference to Fig. 2, assume that $D_x = 0.5$ m, Yee-cell size $\Delta x = \Delta y = \Delta z = D_x/10 = 0.05$ m and time step $\Delta t = \Delta x/2c$. The time for a signal to travel the distance D_x at the speed of light is, therefore, $20\Delta t$. The distance D_x is divided into ten FDTD cells. After 20 time steps, the moving unit cell should have moved the distance D_x. Therefore, moving the unit cell with the speed of light is

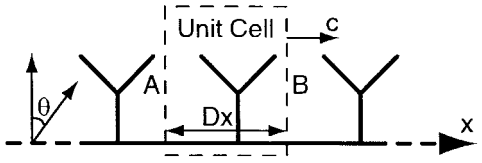

Fig. 2. Side view of the infinite periodic array.

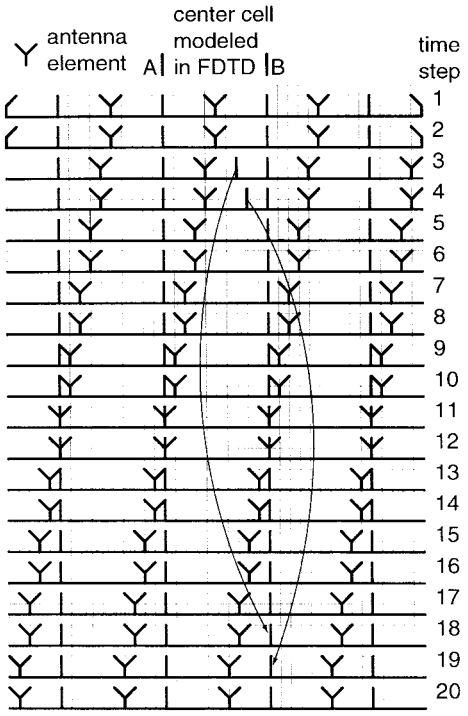

Fig. 3. A 20 time-step cycle in the FDTD simulation. The unit cell is shifted in memory every second time step.

accomplished by shifting the FDTD volume in the computer memory every second time step. Further, the excitation time delay between adjacent unit cells is [(3) repeated]

$$\tau_x = \frac{D_x \sin\theta}{c}. \tag{4}$$

Let N be the excitation time delay τ_x divided by the time step Δt used in FDTD

$$N = \frac{\tau_x}{\Delta t} = \frac{D_x \sin\theta}{c}\,\frac{2c}{\Delta x} = 20\sin\theta = N_0 \sin\theta. \tag{5}$$

In order to reuse earlier computed values the excitation time τ_x must be an integer multiple of the time step Δt. Possible scan angles θ are given by the requirement of N being an integer greater than zero and less than $N_0 = 20$. $N = 0$ corresponds to broadside scanning, which is not possible with the current technique. However, this is not a limitation since at broadside simple time independent boundary conditions may be used (with a nonmoving unit cell). $N = N_0$ corresponds to a scan angle of 90°, which is not possible as explained later. Equation (5) shows that the number of possible scan angles $(N_0 - 2)$ increases with decreasing Δx.

Assume that $N = 15$, corresponding to a scan angle θ of $\arcsin 15/20 = 48.6°$. Fig. 3 shows a $20\,(=N_0)$ time step cycle of the moving unit cell. Only the center cell shown in Fig. 3

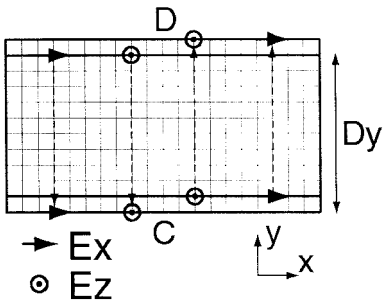

Fig. 4. Implementation of time-independent boundary condition in FDTD for cardinal plane scanning.

is modeled in FDTD. Actually, it is not necessary to model the whole unit cell in FDTD. It is sufficient to model the three FDTD-cells wide part to the left of boundary B, shown at time Step 3. This can be used to reduce the simulation time. At time Step 3, the tangential electric (or magnetic) field is saved in a buffer for use at boundary B at time step $18\,(18 = 3+N)$. At time Step 19 $(19 = 4+N)$, it is not enough to update only the tangential field at boundary B obtained from time Step 4. The reason is that after time Step 18, the FDTD volume is shifted one spatial step Δx and, therefore, it is necessary to update the first layer of electric and magnetic field components (x-, y-, and z components) to the left of boundary B. But those field components are obtained from time Step 4. The algorithm may be implemented by using a circular buffer (with 15 positions in the current example) for the time-delayed field values.

At the start of the FDTD simulation all fields are zero in the moving unit cell. The phase velocity $c/\sin\theta$ of the antenna excitation is always larger than the speed c when $\theta < 90°$ and, as time goes on, the pulse excitation will pass the moving unit cell. A 90° scan angle is not allowed, since the excitation pulse would never disappear. Element currents and voltages are calculated for the element, which happens to be in the moving cell. Therefore, at the end of the FDTD simulation, a simple post-processing of the stored element currents and voltages must be performed in order to obtain the currents and voltages for a particular element in the array. The post-processing is carried out by erasing $N = 15$ time steps of the current and voltage in every $N_0 = 20$ time-step cycle, because they contain no new information. Only $N_0 - N$ new sets of time data are generated in each N_0 time-step cycle. This implies that the simulation time increases with increasing scan angle. After the post-processing, the active impedance may be calculated by a discrete Fourier transform of these currents and voltages.

2) Extension to Two Dimensions: So far, the method described applies to 1-D arrays as in [13]. Extension to 2-D arrays is accomplished by using time-independent boundary conditions. Consider Fig. 1, and assume that the array is scanned in the $y = 0$ plane to an angle θ in the positive x direction. The tangential field at corresponding points on boundaries C and D are then the same and, therefore, a simple time-independent boundary condition applies. Fig. 4 shows how the time-independent boundary condition is implemented in FDTD by wrapping the mesh around itself. Of course, the tangential magnetic field could be used as well.

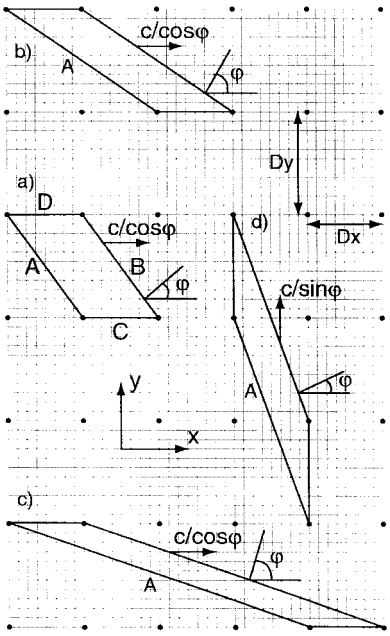

Fig. 5. Some primitive cells in a rectangular lattice with dimension $D_x \times D_y$.

B. Intercardinal Plane Scanning

In this section, intercardinal plane scanning is treated. Although the cardinal scanning technique could be used, it would work only for certain lattice dimensions. Therefore, the method described in this section is a modified version of the cardinal scanning technique. It applies for arbitrary rectangular lattices.

The scanning technique is based on the premise of constructing primitive cells, which are alternative unit cells in the periodic lattice. There are many ways to choose a primitive cell for a given lattice. Fig. 5 shows some primitive cells in a periodic rectangular lattice with dimension $D_x \times D_y$. The shape of the primitive cell determines our intercardinal scan plane, which is perpendicular to the sides A and B. Thus, φ denotes the angle between the x axis and the scan plane. Instead of moving the unit cell with the speed of light c in the scan direction, the unit cell is now moved with a speed larger than c along the x direction. The discrete set of angles φ is easily found to be

$$\varphi = \arcsin \frac{1}{\sqrt{1+\left(\dfrac{D_y}{nD_x}\right)^2}},\ n = 1, 2, 3, \cdots. \qquad (6)$$

Additional angles can be obtained by moving the unit cell along the y axis.

Again, the scanning technique is explained with an example.

3) Example: With reference to Figs. 1 and 5, $D_x = 0.4$ m, $D_y = 0.55$ m. The FDTD cell size $\Delta x = 0.04$ m, $\Delta y = 0.055$ m, and $\Delta z = 0.05$ m. The unit cell shown in Fig. 5(a) is used in the example and the analysis is for the scan direction (θ, φ). The excitation time delay between adjacent unit cells (in the x direction) is

$$\tau_x = \frac{D_x \sin\theta \cos\varphi}{c}. \qquad (7)$$

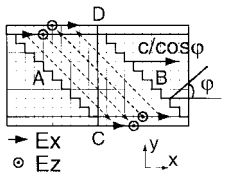

Fig. 6. FDTD implementation of the unit cell in Fig. 5(a).

The FDTD time step Δt should be chosen in a way that makes the moving of the unit cell in the computer memory as easy as possible. A convenient choice of the FDTD time step is

$$\Delta t = \frac{\Delta x}{\frac{2}{\cos\varphi}\, c}. \tag{8}$$

This time step satisfies the Courant–Friedrich–Levy (CFL) stability criterion [see (13)].

As before, define N as the excitation time delay τ_x divided by the time step Δt

$$N = \frac{\tau_x}{\Delta t} = 20 \sin\theta = N_0 \sin\theta. \tag{9}$$

Possible scan angles θ are again given by the requirement of N being an integer greater than zero and less than $N_0 = 20$.

The distance D_x comprises ten FDTD cells and, thus, after $N_0 = 20$ time steps, the moving unit cell will have moved the distance D_x. Therefore, the unit cell must be moved in the computer memory every second time step. The speed of the moving unit cell is independent of Δt and is given by

$$v = \frac{D_x}{N_0 \Delta t} = \frac{D_x}{\frac{\tau_x}{\Delta t \sin\theta}\,\Delta t} = \frac{c}{\cos\varphi} \geq c. \tag{10}$$

This implies that the projection of v onto the φ plane is equal to the speed c. The case $v(\varphi = 0) = c$ corresponds to cardinal scanning. If instead, the unit cell is moved in the positive y direction [Fig. 5(d)] then the unit cell speed would be

$$v = \frac{c}{\sin\varphi} \geq c. \tag{11}$$

The case $v(\varphi = 90°) = c$ corresponds to cardinal scanning.

As before, moving of the unit cell is accomplished by shifting the FDTD volume in the computer memory and the boundary B is updated with saved field values as shown in Fig. 3. The tangential fields at corresponding points on boundary C and D in Fig. 5(a) are the same. Therefore, a simple time-independent boundary condition is used at those boundaries. Fig. 6 shows how the unit cell in Fig. 5(a) is modeled in FDTD. Boundary B is modeled as a staircase (not an approximation).

The whole idea of moving the unit cell is to make (2) unnecessary. However, at first glance, one might suspect that the boundary A in Fig. 5(a)–(d) could be influenced by propagating fields coming from the negative y direction [Fig. 5(a)–(c)] or from the negative x direction [Fig. 5(d)] because of the slope of the boundary A. However, this does not happen, since the projected unit cell speed v onto the φ plane is equal to the speed of light.

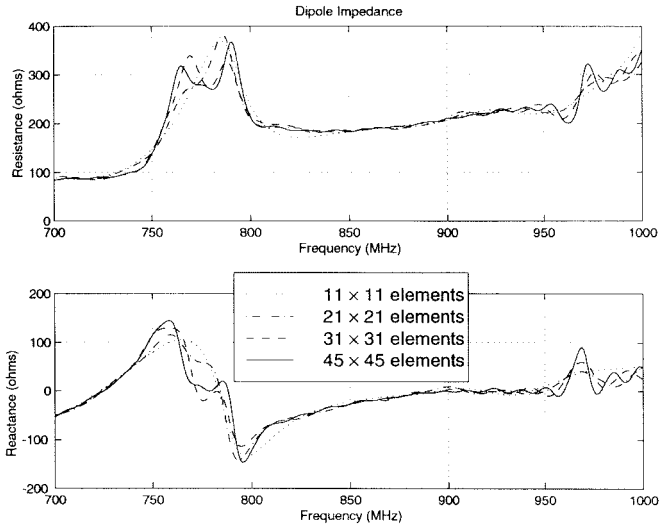

Fig. 7. Scan direction $\theta = 44.4°$, $\varphi = 71.0°$. Active impedance for the finite array calculated with different number of antenna elements.

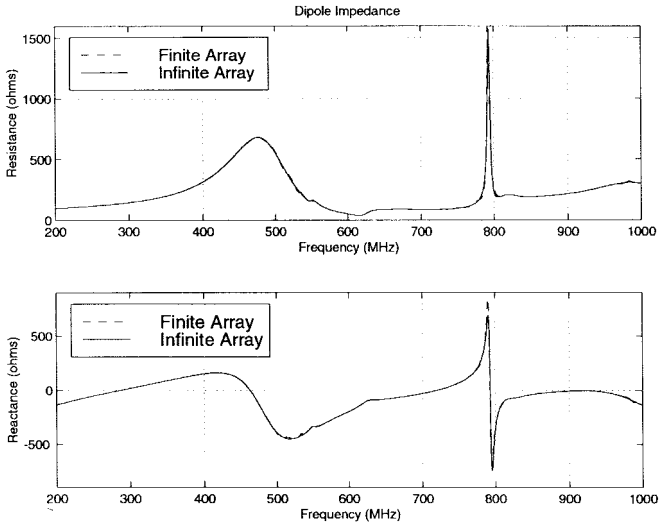

Fig. 8. Active impedance for the scan direction $\theta = 11.5°$, $\varphi = 0°$. The first grating lobe enters visible space at 557 MHz and others at 625 and 803 MHz.

IV. Validation

Using the new technique we calculated the active impedances for an infinite periodic 2-D phased array scanned in both cardinal and intercardinal planes. Validation was performed via the "element-by-element" approach, i.e., by a conventional FDTD simulation of a corresponding large finite array.

A. Absorbing Boundary Condition on Nonperiodic Boundaries

Nonperiodic boundaries, i.e., boundaries in the positive and negative z directions, were truncated by Berenger's perfectly matched layer (PML) [14]. The PML layer had a thickness of 12 FDTD cells and a quadratic profile with a reflection coefficient for normal incidence of 10^{-6}. In the conventional FDTD simulation, PML was used to truncate all six boundaries with the same layer characteristics as above.

TABLE I
SIMULATION DATA FOR SIX DIFFERENT TEST CASES

Simulation Data						
Scan direction		Time step Δt in FDTD	Speed of unit cell	Simulation time (minutes)		
θ	φ			infinite array (t1)	finite array (t2)	t2/t1
11.5^0	0.0^0	$\Delta x/2c$	c	0.9	1440	1600
64.2^0	0.0^0	$\Delta x/2c$	c	7.0	1140	163
64.2^0	20.0^0	$\Delta y \sin\varphi/c$	$c/\sin\varphi$	11.8	1325	112
30.0^0	36.0^0	$\Delta x \cos\varphi/2c$	$c/\cos\varphi$	3.6	2990	831
53.1^0	55.5^0	$\Delta x \cos\varphi/c$	$c/\cos\varphi$	5.0	2020	404
44.4^0	71.0^0	$\Delta x \cos\varphi/c$	$c/\cos\varphi$	7.7	3410	443

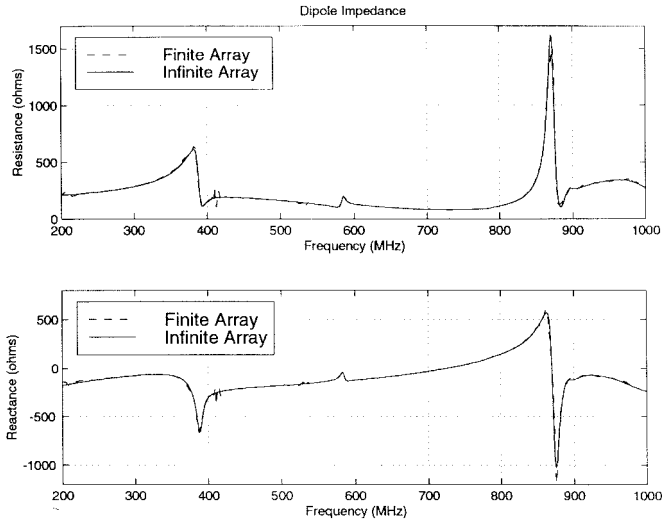

Fig. 9. Active impedance for the scan direction $\theta = 64.2°$, $\varphi = 0°$. The first grating lobe enters visible space at 395 MHz and others at 588, 789, and 888 MHz.

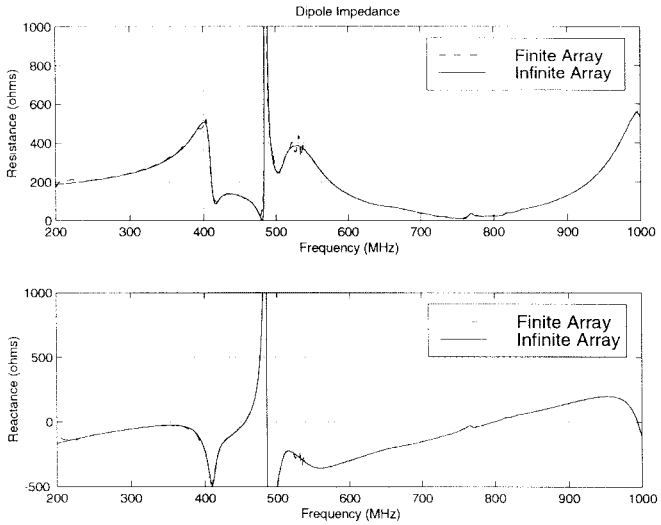

Fig. 10. Active impedance for the scan direction $\theta = 64.2°$, $\varphi = 20.0°$. See Fig. 11 for the impedance around 470–510 MHz. The first grating lobe enters visible space at 417 MHz and others at 506, 649, 794, 835, and 840 MHz.

When the FDTD volume was shifted in the computer memory in order to move the unit cell, the PML layer was also shifted and updated with time-delayed values from a buffer.

Initially, a second-order absorbing boundary condition (first order at corners and edges) was used to truncate nonperiodic boundaries. Sometimes, this led to numerical instability. However, after implementation PML, there have been no indications of numerical instability even when the simulations were run for very long times (300 000 time steps).

B. Test Cases

An infinite dipole array was used as test case. The following data are common to all simulations: $D_x = 0.4$, $D_y = 0.55$ m. FDTD cell size $\Delta x = 0.04$ m, $\Delta y = 0.055$ m, and $\Delta z = 0.05$ m. The dipoles, pointing in the y direction and fed at the midpoints were modeled by setting nine collinear electric field components (E_y) along subsequent FDTD cells equal to zero. The smallest distance between the dipoles and the PML layer was five FDTD cells for both the finite and the infinite array. The frequency spectrum considered was 200–1000 MHz. The excitation pulse used was

$$v(t) = e^{-(1/2)((t-8/\Delta\omega)\Delta\omega)^2} \sin(\omega(t - 8/\Delta\omega)) \qquad (12)$$

where $\Delta\omega = 2\pi 300$ MHz and $\omega = 2\pi 550$ MHz. The finite array contained $45 \times 45 = 2025$ dipoles. This is a large number of dipoles, but as can be seen from Fig. 7, the impedance clearly changes when the number of dipoles is increased. The active impedance is calculated for the center element of the array.

The time step used satisfies the CFL stability criterion.

$$\Delta t \leq \frac{1}{c\sqrt{\dfrac{1}{(\Delta x)^2} + \dfrac{1}{(\Delta y)^2} + \dfrac{1}{(\Delta z)^2}}}. \qquad (13)$$

Table I contains simulation data for the different test cases. Two simulations were performed in the cardinal plane ($\varphi = 0$) and four simulations were performed in intercardinal planes. Table I shows that the simulation time for the infinite array increases with increasing scan angle θ, which is expected as explained earlier.

In all simulations, the computer used was a 300-MHz Intel Pentium II pc (dual processors) equipped with 512 MB of memory.

1) Modeling of the Antenna Feed: A simple feed model which incorporates a series resistance of 50 Ω was used for the dipoles [15]. This feed model reduced the simulation time significantly.

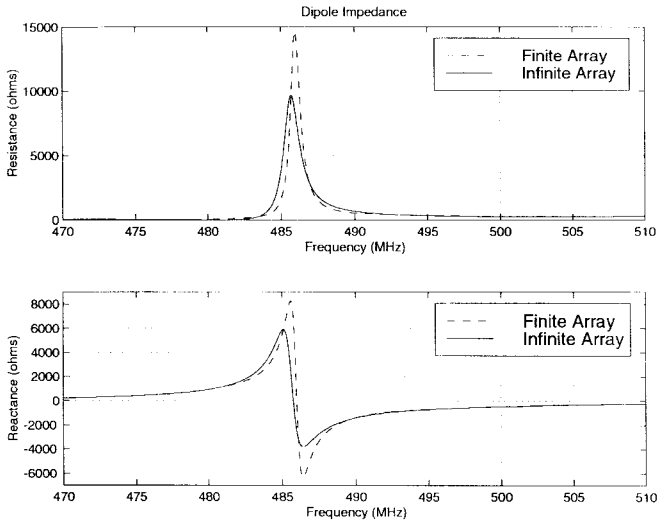

Fig. 11. Active impedance for the scan direction $\theta = 64.2$, $\varphi = 20.0°$. This is Fig. 10 magnified around 470–510 MHz.

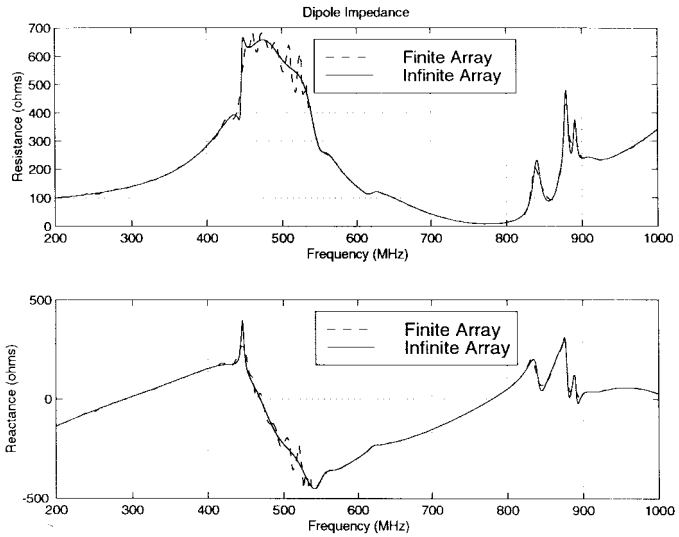

Fig. 12. Active impedance for the scan direction $\theta = 30.0°$, $\varphi = 36.0°$. The first grating lobe enters visible space at 451 MHz and others at 551, 618, 879, 897, 903, and 908 MHz.

The antenna voltage $V(t)$ was calculated as $-E_y \Delta y$, where E_y is the electric field in the feed gap. The total antenna current $I_{\text{tot}}(t)$ at the feed point was calculated from

$$I_{\text{tot}}(t) = \oint \mathbf{H} \cdot d\mathbf{l}. \tag{14}$$

which means that the displacement current is included in $I_{\text{tot}}(t)$. If desired, it is possible to remove the displacement current from (14) as shown in [16].

The active impedance is calculated from the discrete Fourier transforms of $V(t)$ and $I_{\text{tot}}(t)$. For the test cases in this paper, it is important to compensate for the time difference $\Delta t/2$ between the voltage and current. Therefore, in the active impedance calculation, the Fourier transformed voltage $V(\omega)$ was multiplied by an appropriate phase factor as shown

$$Z(\omega) = \frac{V(\omega) e^{-j\omega \Delta t/2}}{I_{\text{tot}}(\omega)}. \tag{15}$$

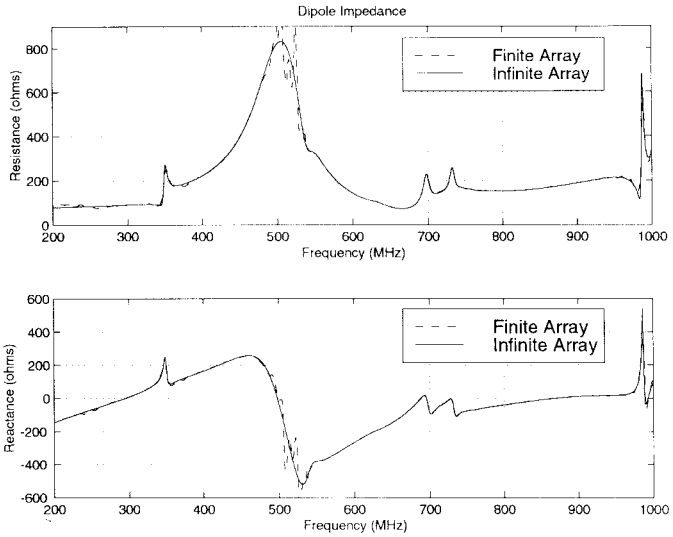

Fig. 13. Active impedance for the scan direction $\theta = 53.1°$, $\varphi = 55.5°$. The first grating lobe enters visible space at 352 MHz and others at 540, 622, 704, and 736 MHz.

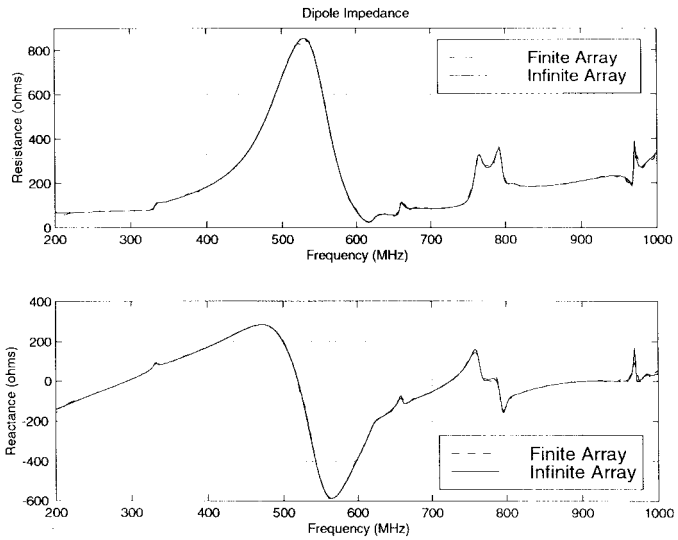

Fig. 14. Active impedance for the scan direction $\theta = 44.4°$, $\varphi = 71.0°$. The first grating lobe enters visible space at 334 MHz and others at 623, 667, 767, 799, and 978 MHz.

Ignoring this phase factor results in a negative resistance of about $-100\ \Omega$ around 482 MHz in Fig. 10 for both the finite and the infinite array.

2) Cardinal Plane Scanning: Figs. 8 and 9 shows the simulation results for cardinal plane scanning. The agreement between the finite and the infinite array is excellent.

3) Intercardinal Plane Scanning: Figs. 10–14 shows the simulation results for intercardinal plane scanning. In some cases, e.g., Figs. 12 and 13 at about 500 MHz, the impedance of the finite array oscillates around the infinite array impedance. These oscillations decrease if more antenna elements are used. Therefore, they are most likely an effect caused by the finite number of elements. More interesting is the $\theta = 64.2°$, $\varphi = 20.0°$ scan case in Figs. 10 and 11. At 482 MHz, the impedance is very near zero and at 486 MHz the impedance is very high. This cannot be a regular blind

spot since a grating lobe has already entered visible space at 417 MHz. However, it does indicate more or less total power reflection and thus implies a main lobe and grating lobe of low or zero amplitude. The next grating lobe enters visible space at 506 MHz and is therefore unlikely to be associated with the strange impedance behavior.

V. Summary

A new technique for FDTD analysis of obliquely scanning, pulsed-array antennas has been presented. It reduces the computational volume to a single unit cell of the array and, therefore, is computationally highly efficient. The technique has been successful applied to a 2-D array of dipoles scanned in both cardinal and intercardinal planes.

References

[1] N . Amitay, V. Galindo, and C. Wu, *Theory and Analysis of Phased Array Antennas.* New York: Wiley, 1972.

[2] J. Roden, S. Gedney, M. Kessler, J. Maloney, and P. Harms, "Time-domain analysis of periodic structures at oblique incidence: Orthogonal and nonorthogonal FDTD implementations," *IEEE Trans. Microwave Theory Tech.*, vol. 46, pp. 420–427, Apr. 1998.

[3] Y. Kao and R. Atkins, "A finite difference-time domain approach for frequency selective surfaces at oblique incidence," in *IEEE Antennas Propagat. Soc. Int. Symp. Dig.*, 1996, pp. 1432–1435.

[4] J. Ren, O. Gandhi, L. Walker, J. Fraschilla, and C. Boerman, "Floquet-based FDTD analysis of two-dimensional phased array antennas," *IEEE Microwave Guided Wave Lett.*, vol. 4, pp. 109–111, Apr. 1994.

[5] M. Veysoglu, R. Shin, and J. Kong, "A finite-difference time-domain analysis of wave scattering from periodic surfaces: Oblique incidence case," *J. Electron. Waves Applicat.*, vol. 7, no. 12, pp. 1595–1607, 1993.

[6] A. Alexanian, N. Kolias, R. Compton, and R. York, "Three-dimensional FDTD analysis of quasioptical arrays using Floquet boundary conditions and Berenger's PML," *IEEE Microwave Guided Wave Lett.*, vol. 6, pp. 138–140, Mar. 1996.

[7] M. Celuch-Marcysiak and W. Gwarek, "Spatially looped algorithms for time-domain analysis of periodic structures," *IEEE Trans. Microwave Theory Tech.*, vol. 43, pp. 860–865, Apr. 1995.

[8] P. Harms, R. Mittra, and W. Ko, "Implementation of the periodic boundary condition in the finite-difference time-domain algorithm for FSS structures," *IEEE Trans. Antennas Propagat.*, vol. 42, pp. 1317–1324, Sept. 1994.

[9] D. Prescott and N. Shuley, "Extensions to the FDTD method for the analysis of infinitely periodic arrays," *IEEE Microwave Guided Wave Lett.*, vol. 4, pp. 352–354, Oct. 1994.

[10] W. Tsay and D. Pozar, "Application of the FDTD technique to periodic problems in scattering and radiation," *IEEE Microwave Guided Wave Lett.*, vol. 3, pp. 250–252, Aug. 1993.

[11] C. Chan, S. Lou, L. Tsang, and J. Kong, "Electromagnetic scattering of waves by random rough surface: A finite-difference time-domain approach," *Microwave Opt. Technol. Lett.*, vol. 4, no. 9, pp. 355–359, Aug. 1991.

[12] E. Navarro, B. Gimeno, and J. Cruz, "Modeling of periodic structures using the finite difference time domain method combined with the Floquet theorem," *Electron. Lett.*, vol. 29, no. 5, pp. 446–447, Mar. 1993.

[13] H. Holter and H. Steyskal, "Broadband FDTD analysis of infinite phased arrays using periodic boundary condition," *Inst. Elect. Eng. Electron. Lett.*, vol. 35, no. 10, pp. 758–759, 1999.

[14] J. Berenger, "Three-dimensional perfectly matched layer for the absorption of electromagnetic waves," *J. Comput. Phys.*, vol. 127, pp. 363–379, 1996.

[15] R. Luebbers and H. Langdon, "A simple feed model that reduces time steps needed for FDTD antenna and microstrip calculations," *IEEE Trans. Antennas Propagat.*, vol. 44, pp. 1000–1005, July 1996.

[16] H. Holter, "Antenna feed modeling in the finite difference time domain method," Master's thesis, Ericsson Radio Syst. AB and Royal Inst. Technol., Nov. 1996.

Henrik Holter received the M.S. degree from the School of Electrical Engineering, Royal Institute of Technology (KTH), Stockholm, Sweden, in 1996, with the distinction of Best Graduate of the Year. He is currently working toward the Ph.D. degree at the Department of Electromagnetic Theory, KTH.

His research interests include broad-band antenna elements for phased arrays and numerical electrodynamics. In 1999, he spent a six-month visit at the Antenna Laboratory, University of Massachusetts, Amherst, participating in research on tapered-slot antenna elements for phased arrays. He served the Swedish Navy from 1986 to 1996 with a Lieutenant degree (Swedish "Kapten") in electrical engineering.

Hans Steyskal (M'76–SM'91–F'96) received the Civ.Ing., Tekn.Lic., and Tekn.Dr. degrees in electrical engineering from the Royal Institute of Technology (KTH), Stockholm, Sweden, in 1963, 1970, and 1973, respectively.

In 1962, he joined the Swedish National Defense Research Institute (FOA), where he worked on microwave radiation and scattering problems. In 1980, he gave up his position as Chief of the Section for Field and Circuit Theory and moved to the United States. He now pursues his interests in electromagnetics and applied mathematics at the Air Force Research Laboratory (formerly Rome Air Development Center), Hanscom AFB, MA. Since 1996 he has also held a part-time position as an Adjunct Professor in Antenna Technology at KTH.

Dr. Steyskal has served two terms as an Associate Editor for the IEEE Transactions Antennas and Propagation in the area of array antennas.